Highly Multiplexed Confocal Fluorescence Lifetime Microscope Designed for Screening Applications

Nehad Hirmiz, Anthony Tsikouras, Elizabeth J. Osterlund, Morgan Richards, David W. Andrews, and Qiyin Fang

***Abstract* —Protein-protein interactions can be measured in live cells, at nanometer scale, using Fluorescence Lifetime Imaging Microscopy (FLIM) enabled Förster Resonance Energy Transfer (FRET). There are growing interests in exploring protein-protein interactions in drug discovery applications. Traditional single point confocal microscopes, however, are slow and unsuited to small molecule screening, especially when combined with FLIM-FRET. We developed a 32×32 multiplexed confocal microscope, which employs a single-photon avalanche photodiode array with time gating capabilities for rapid FLIM acquisition. It has been demonstrated that such multiplexing technique can capture a 960×960 pixel multi-channel confocal fluorescence lifetime images in less than 1.5 seconds. Binding curves of two Bcl-2 family proteins: Bcl-XL and Bad were generated in live cells imaging experiments. The results show that the small molecule inhibitor A-1131852 is a more effective compound for disrupting Bcl-XL binding to Bad than ABT-263, which demonstrated the feasibility of screening of protein-protein interactions in high density well-plates.**

***Keywords*—Fluorescence lifetime Imaging (FLIM), single photon avalanche diode (SPAD), time gated sensor, Microscopy.**

I. Introduction

CELLULAR mechanisms are carried out by large protein-protein interaction networks. Targeting a specific interaction with a small molecule may alter this network, lead to a biological change, which may be useful for personalized medicine [1], [2]. Knowing a compound specifically disrupts a protein-protein interaction helps biologists understand the mechanism and predict therapeutic outcomes. In 2016 FDA approval was granted for use of ABT-199, a small molecule that binds the protein Bcl-2 and prevents interactions with other proteins in the cell, for treatment of chronic lymphocytic leukemia [3]. Now many protein-protein interactions are being explored as potential therapeutic targets.

In traditional drug development, thousands of small molecules are screened to identify compounds that give a desired readout. Methods used for these primary screens typically yield false positives and hit compounds need authentication in secondary screening [4-5]. Choosing the appropriate method to measure compound binding selectivity reduces the chance of failure in later stages of drug development, e.g animal models and clinical trials. There are several biophysical approaches to measure binding [6]: Isothermal Titration Calorimetry (ITC) measures enthalpic changes due to protein-protein or protein-drug binding [7]; surface plasmon resonance (SPR) measures binding by examining the accumulation of materials on surface immobilized target molecules [8]. However, these methods are done in a test tube and require purification of the target proteins, which may not be attainable.

An alternative is to express two proteins in a cell. Fusion of the proteins of interest to fluorophores allows visualization by fluorescence microscopy. An interaction between the two fusion proteins can be detected by measuring Förster resonance energy transfer (FRET) between the two fluorophores, where the rate of energy transfer is inversely proportional to the sixth power of the distance separating the two proteins. This dependency makes FRET a powerful molecular ruler because small changes in the distance result in large changes in the rate of energy transfer. Disruption FRET between two fusion-proteins of interest is a direct way to measure a compound is on-target.

FRET can be measured by a few different approaches [9]. The sensitized emission approach evaluates the increase in the acceptor intensity due to FRET [10]. Alternatively, the acceptor fluorophore can be photobleached, preventing FRET, and the difference in the donor fluorescence intensity before and after photobleaching can be used to quantify FRET [11]. These intensity-based approaches require multiple measurements to correcting for spectral bleed through. The signal to noise must be high or there will be uncertainty in FRET estimation. Thus, measurement accuracy strongly depends on the concentration of fluorescent molecules in the excitation volume.

Manuscript received on January 25, 2020. This work was supported in part by the Natural Science and Engineering Research Council (NSERC) of Canada, Canadian Foundation of Innovation, the Ontario Research Fund, and the Canada Research Chairs program.

N. Hirmiz, and Q. Fang (qiyin.fang@mcmaster.ca) are with the School of Biomedical Engineering at McMaster University, Hamilton, Ontario, L8S 4L7, Canada

A. Tsikouras, M. Richards, and Q. Fang are with the Department of Engineering Physics at McMaster University

E. J. Osterlund and D. W. Andrews are with the Department of Biochemistry, Sunnybrook Research Institute, University of Toronto, Toronto, Ontario, M4N 4L7, Canada

Fluorescence lifetime imaging microscopy (FLIM) can measure FRET (FLIM-FRET) independent of concentration [12]. Single-photon or time-gated detectors are used to measure the arrival time of photons emitted by the donor fluorophore. The arrival time distribution can be used to determine the fluorescence lifetime, which is the average time a population of fluorescent molecules remains in the excited state before returning to ground state. Fluorescence lifetime is sensitive to environmental changes. For example, in the presence of an acceptor fluorophore, FRET provides the donor molecule with a new route to relax back to the ground state. Thus, FRET causes a decrease in the fluorescence lifetime of the donor. Unlike intensity-based approaches, there is no requirement for spectral correction. When combined with confocal, FLIM-FRET can be used to measure dynamic protein-protein interactions in 3 dimensions in live cells, which is important in applications such as drug discovery [13].

Traditional confocal FLIM-FRET is time-consuming and not suitable for high throughput screening [14]. Typical pixel dwell times on the order of 100 microseconds to 0.5 milliseconds. For a 256×256 pixels this results in acquisition times in the range of 6.5 seconds to 35 seconds. Confocal scanning creates sub-cellular level resolution interaction maps, which can be useful for determining how and where proteins function. Hundreds to thousands of photons must be collected at each pixel to accurately estimate the fluorescence lifetime. A single excitation point is scanned across the sample to create the image. In order to increase scan speed, the excitation and/or detection can be multiplexed [15]-[17]. Multiplexing refers to parallel excitation and/or detection of more than one point minimally, across the image sample. Confocal multiplexing methods, such as the spinning disk confocal offer a faster solution. However, spinning disk imaging requires spreading the collected fluorescence signal on a dense array detector such as a CCD or CMOS, and cannot be coupled to a single photon detector. Furthermore, spinning disk FLIM deploys time-gated multichannel plates (MCPs), which have limited temporal resolution and can only acquire a single time-gate per scan. Spinning disk FLIM systems are currently not commercially available and are built by specialized research groups [18]. To push FLIM-FRET imaging into the early screening pipeline, we need a highly multiplexed confocal system that can be coupled to single-photon counting arrays, which are a rapidly maturing and increasingly affordable technology.

To address this challenge, we developed a multiplexing technique that de-scanned the fluorescence array signal such that it is stationary when reaching the detector. The degree of multiplexing in our system is comparable to that of the spinning disk. However, our fixed array collection design allows us to couple to not only dense detectors but also sparse single-photon avalanche diode (SPAD) and fibre optic arrays for signal collection. In our previous work, we demonstrated how a 2D-1D fibre bundle can be used to couple our multiplexed microscope to a streak camera [19]. We addressed the limitations of the multiplexed confocal streak system for live cell imaging. In summary, the low coupling efficiency to the fibre array prevented rapid FLIM acquisition, while crosstalk effects limited the scalability of the design to 10×10 multiplexing.

In this work, improvements made on our previously published design will be discussed and demonstrated. The degree of multiplexing can be increased by ten-fold by using 32×32 excitation points to scan the sample and coupled the collected fluorescence emission to a time-gated single-photon counting SPAD array. By eliminating the fiber optic bundle and directly coupling the emission light to a SPAD array, we can achieve significantly higher coupling efficiency. Our multiplexing solution coupled to the SPAD array detector offers a high resolution and a rapid imaging platform suitable for fast confocal FLIM imaging. Finally, we measure the interaction between two proteins from the Bcl-2 family and demonstrate complex disruption by 2 known targeted small molecules in live cells.

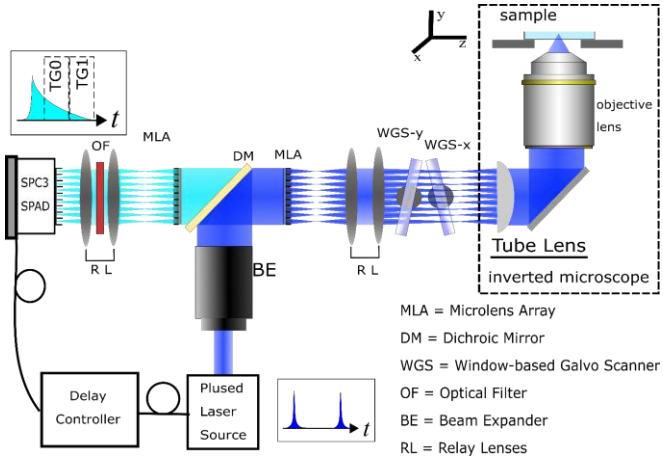

Fig. 1. The Multifocal Confocal FLIM Setup. Schematic diagram of our multiplexed confocal system attached to an inverted commercial microscope.

II. Experimental Setup

The schematics of the multiplexed confocal FLIM microscope is shown in Fig. 1. Excitation multiplexing is achieved by generating a grid of 32×32 excitation points, using a pair of microlens arrays (MLAs). A picosecond pulsed laser (470nm, LDH-P-C-470, PicoQuant, Berlin-Adlershof, Germany), was chosen for excitation of both cyan (mCerulean3) and yellow (Venus) fluorescent proteins simultaneously. Excitation light that leaks past the dichroic and emission filter can be temporally gated out by the SPAD detector. A beam shaper is used to expand the excitation light such that it can cover a 32×32 MLA (APO-Q-P300-R1.83, Advanced Microoptic Systems, Saarbrücken, Germany), which has an anti-reflection coating. A dichroic mirror is used to reflect excitation light into the first MLA. This results in a foci array at the focal point of the MLA, which is then relayed through a pair of lenses to the conjugate plane of the side excitation port of an inverted fluorescence microscope (DMI 6000B, Leica, Wetzlar, Germany).

A pair of refraction window-based galvo scanners are positioned near the conjugate plane of the microscope to scan

the 32×32 excitation foci in parallel along the x and y directions in a step-and-stop raster pattern [20]. The tube lens then relays the image to a 40× oil immersion objective (HC PL APO 40x/1.30 Oil CS2, Leica) and focuses the excitation array onto the sample.

The fluorescence emission returns along the same light path, passing the first MLA, which collimates the signal. The collected fluorescence light passes through the dichroic mirror and is then projected onto a second MLA to recreate the grid of foci. Finally, the signal foci array is collected by an SPAD detector (SPC3, Micro Photon Devices, Bolzano, Italy) with matching pixels. The SPAD array detector is consisting of 64×32 individual SPADs, half of which (32x32) are actively used in our design. Each pixel has a 30 µm active-area diameter with average quantum efficiency ~30% (25% at 320 nm, 50% at 400 nm, and 14% at 650 nm). The pixel pitch is 150 µm (3.14% fill factor). The detector can capture two-time gates simultaneously. The minimum stable size for each gate is 2 ns and the observation window is 16 ns. Detection can be performed at a count rate of up to 50 Mcps and dead-time as short as 20 ns. The detector can be set to perform background detection and rapid lifetime determination on-chip [21]. It should be noted that we used a prototype device on loan from the manufacturer. We did not implement the simultaneous two-gate detection or on-chip processing feature due to firmware compatibility issues. Instead, each time gate was acquired separately with background subtraction and lifetime determination done off-chip.

A 2:1 pair of relay lenses, match the 300um pitch MLA to the 150µm pixel pitch of the SPAD array. An optical emission filter (FF01-483-25, Semrock, Rochester, NY) is positioned between the relay lenses to reject any excitation light that had leaked though the system. The SPAD array has a large active pixel area (30 um) which makes it easier to couple to in a multiplexed system. The size of each spot at the detection plane was measured to be ~20 µm, using a dense CMOS camera before placing the SPAD array detector. The sensor is mounted on a 3-axis stage constructed by combining three crossed-roller bearings stages (Thorlabs, XR25, NJ). The alignment is achieved by ensuring that maximum counts are observed across the entire sensor. Rotational misalignment can be easily detected as the photon count changes across the sensor are out of synchronization. To help visualize this effect using our software, we color the pixels red when they reach a specified threshold.

Direct coupling to the SPAD array ensures optimized collection efficiency. We found this setup to be stable over time. The emitted photons are collected between two separate time-gates. Accurate estimation of fluorescence lifetime requires optimizing the position of these gates with respect to the excitation pulse.

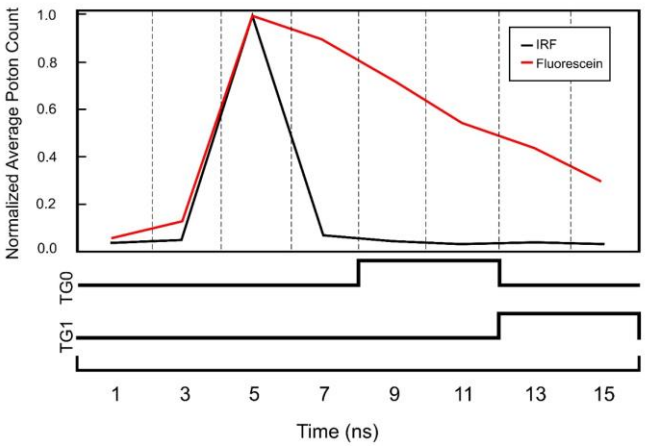

Fig. 2. Time-gates position and size. Normalized profile IRF (black) and Fluorescein in 0.1mM NaOH (red). For rapid lifetime imaging, we choose two time-gates (TG0 and TG1). The position of the two 4ns time-gates is also indicated above the time axis. The permitted observation window for the SPC3 is 16 nanoseconds presented as the time axis limits.

Rapid fluorescence lifetime determination is achieved by examining the ratio of photons collected within the two time-gates (TG0 and TG1). Prior to FLIM imaging, we optimized the location of the time-gates. We first made sure that the collection windows do not include the instrument response function (IRF), measured using a quenched fluorescein sample with a 27 ps fluorescence lifetime, to determine the gate position (Fig. 2). The quenching was achieved by increasing the pH to 10, adding 12M quenching salt NaI and preparing the fluorescein solution at a high concentration (510 µM) to maximize collisional quenching. The sample preparation and lifetime estimation are discussed in detail in [22] and we provide a step by step recipe in [23]. A 2 ns window temporally shifted at 2 ns intervals, was used to precisely locate the IRF position. The delay between the pulsed laser and the SPC3 SPAD array was then adjusted such that the start of the first time-gate was outside the IRF collection region. We also considered the size of the observation window permitted by the SPC3 SPAD detector (a 16 nm collection window) in choosing appropriate gate widths. Two non-overlapping equal size gates, 4 ns each, were chosen (Fig. 2). The size of a single gate is comparable to the longest expected fluorescent lifetime that was measured (fluorescein, 4.0 ns).

III. Materials and Methods

A. Live Cell Sample Preparation

In live cell imaging experiments, an MCF-7 (PMID: 3790748) breast cancer cell line model was used. The cells have been bioengineered to expresses a protein (Bcl-XL) with the donor fluorophore (mCerulean3) fused to its N-terminus [23, 24]. The sequence of Bcl-XL protein was cloned downstream of mCerulean3 in the DNA vector (EGFP-C3 backbone, where EGFP is replaced with mCerulean3). This vector contains a gene for Neomycin resistance, so upon treatment with Neomycin sulphate (G418) only cells that have taken up this vector survived. Cells were maintained in

selection media for at least 2 weeks, during which time, the foreign DNA may have randomly integrated into the cell genome, for stable expression of the fusion protein. Sorting by flow cytometry was performed to select a narrow range of expression levels of mCerulean3-Bcl-XL (DNS).

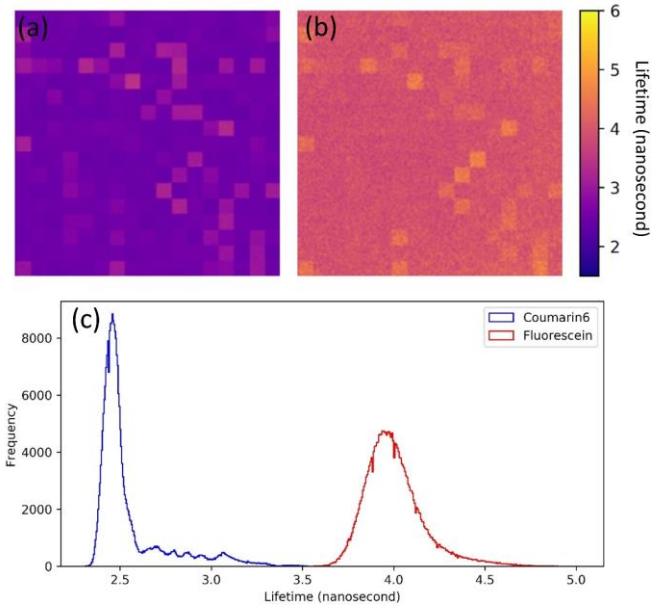

Fig. 3. Lifetime maps of (a) Fluorescein in 0.1M NaOH, 10uM, (b) Coumarin6 in ethanol 10uM. (c) Lifetime distributions for Coumarin-6 and Fluorescein reconstructed from (a) and (b) respectively. (a) and (b) are 184×184 µm cropped regions of interest.

All cell lines were incubated at 37˚C, 5% v/v CO2. Cell handling was performed in a biosafety level 2 cabinet. MCF7-mCerulean3-Bcl-XL human breast cancer cells [23] were passed 1 in 6, every 3-5 days. Cells were maintained in Alpha-MEM complete media (10% FBS, 1% Penstrep) + G418 (400-130-IG, Wisent, Quebec). HEK-293 cells were passed 1 in 10, every 3 days and maintained in DMEM complete media (10% FBS, 1% MEM-NEAA, 1% Penstrep).

On day 1, media from 10cm dish of confluent cells (80% covered dish) was aspirated. Cells are washed with 3ml PBS. PBS was aspirated and 1ml of 2x Trypsin was added and incubated for 2 minutes. Cells should lift off the plate and can be pipetted up/down to eliminate clumps. Then 1ml of resuspended cells was diluted in 5ml Alpha-MEM complete media. A haemocytometer was used to count cells. The cells were then diluted to 160cells/ µl, and 25µl volume was added to each well (4000 cells per well). The well plate was left at room temperature for 15 minutes, before returning them to the incubator. This allows the cells to settle at the bottom after the wash step. Cells were incubated overnight (up to and no longer than 24 hours).

On day 2, cell transfection was carried out. First reagents were warmed in 37˚C water bath: 5ml aliquot of Opti-MEM, TransIT X2 transfection reagent (MIR 6005, Mirus, WS), Alpha-MEM complete media and DNA constructs (including Acceptor-fusion protein of interest and controls). Several 1.5ml tubes were labelled with the name for each transfection reaction. In each tube, a 9µl OPTI-MEM (31985-070, Gibco, CA), 1µl transfectant DNA (100ng/ul) and 0.3µl TransIT-X2 were added. Each tube was briefly vortexed, centrifuged by 'burst', then incubated for 15 minutes at room temperature. 50µl of Alpha-MEM complete media was added to each transfection reaction and gently pipetted up/down. 25µl of this transfection reaction was added to each well, on top of the 25 of cells seeded the previous day. Note that each transfection reaction is enough to transfect 2 wells with 10µl extra to account for any pipetting error. For 'untransfected' control wells create a 'mock' transfection: add 25µl of media plus 0.3µl transfection reagent (with no DNA). Note that some proteins may not be expressed as quickly as others. Transfected cells were incubated up to 48 hours prior to imaging.

Wait 3-5 hours then media should be replaced with 50 µl fresh media to reduce the toxicity of the transfection reagent. This is the ideal time to treat with a drug prior to complex formation. BH3 mimetics were diluted 1:1000 (stock solution was 5mM A-1331852 (CT-A115, Chemietek, IN) and 20mM ABT-263 (S1001, Selleckchem, TX) in media and used to treat selected wells. A control dilution of the 1:1000 DMSO in media is made for the 'untreated' wells. Do not touch the bottom of the well to avoid washing cells off; tilt the plate on one side and pipette out media from bottom left corner.

B. FLIM Acquisition

The FLIM Acquisition was controlled by a homebuilt interface, written in C++ (Visual Studio 2015). Time-gate position, width and number of gates were specified and relayed to the SPAD detector using the API provided. The number of steps per scan were also adjusted and relayed to the galvo drivers. For FLIM imaging the SPAD was set in a single time-gated mode. Two 4 nanosecond time-gates (mCerulean3 collection) or a single 8 nanosecond time-gate (Venus collection) were used. A delay generator (Picosecond Delayer, Microphoton Devices, Bolzano, Italy) was used to add a 4 ns delay between the two-gate acquisitions (delay controller Fig. 1). The delay trigger was controlled through an API and scanning is performed such that the photons are collected for the entire sample at each time-gate.

The 470nm diode laser was the excitation source for all FLIM experiments reported here. The emission channel was set by changing the emission filter. For quenched Fluorescein, Fluorescein (2321-07-5, Sigma Aldrich, MO), Coumarin-6 (38215-36-0, Sigma Aldrich, MO) and the *Convallaria* (*Convallaria Majalis*, Leica) standard samples, a 484-25 bandpass emission filter was used. For live cell FLIM-FRET measurements, the mCerulean3-Bcl-XL emission was collected using the 483-25 bandpass filter (donor channel), while the Venus labelled proteins were imaged using 535-40 bandpass filter (acceptor channel). The 470nm excitation was used to excite the Venus labelled proteins as well. Plotting the intensity of mCerulean3-Bcl-XL only samples in donor channel against acceptor channel indicated a linear cross talk, which is corrected for during data analysis (DNS).

C. Image Processing and Lifetime Estimation

The photons collected for each time-gate were saved into a separate image. For a two-gate scan, the two images were first combined to get a total intensity image, which was used to create a background mask. Pixels with low photon counts were excluded from the analysis. The mask was applied to both gated intensity images. For live cell FLIM imaging, a 5×5pixel binning was applied to improve lifetime estimation. Masked pixels were excluded from the binning in the analysis.

Rapid lifetime determination (RLD) method was used to estimate the fluorescence lifetime. The lifetime image was calculated using:

$$\tau_{RLD} = \Delta t / \ln (D_0/D_1) \quad (1)$$

Where Δt is the temporal separation between the beginning of the two gates, D_0 and D_1 are the photon count images at the first and second time-gates respectively.

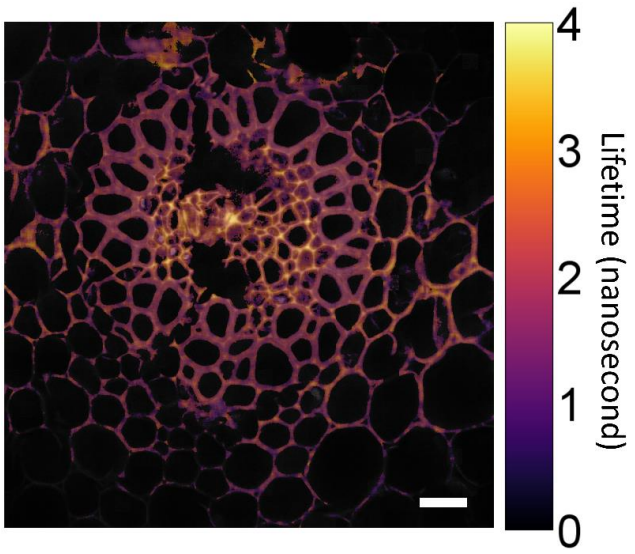

Fig. 4. Photon weighted FLIM confocal image of Convallaria. Scale bar 30 µm. A threshold mask is applied, pixels with photon count < 20 are set to zero.

D. FRET Efficiency and Apparent Binding Affinity

Stable expression of mCerluean3-Bcl-XL in the cells results in similar expression levels of the protein from one cell to another. Transient transfection of Venus-Bad, on the other hand, results in more variable expression levels among the cells. This variation in the acceptor to donor (acceptor:donor) ratio leads to variation in FRET observed from one cell to the other. Sampling this variation is important for generating full binding curves.

Each measured pixel was the result of the signal collected from the confocal volume at that point in the sample. Pixels with a high acceptor:donor ratio have higher probability the donor will come in close proximity the acceptor for FRET to occur. The acceptor: donor ratio was calculated by dividing the acceptor intensity image over the donor intensity image. This ratio was plotted as a function of apparent FRET efficiency calculated using:

$$FRET\ Efficiency\ \% = (1 - \tau_D/\tau_{DA}) \times 100\% \quad (2)$$

Where the τ_D and τ_{DA} are the fluorescence lifetimes of the donor in the absence and presence of the acceptor, respectively. τ_D was determined by examining the fluorescence lifetime of untransfected MCF-7 cells expressing mCerulean3-Bcl-XL. The plot of FRET efficiency as a function of acceptor:donor ratio was used to extract the apparent Kd. Data was binned based on the acceptor:donor ratio for final binding curves, and fit using a single site hill equation:

$$Y = (Bmax\ X)/(K_d + X) \quad (3)$$

Where Y is the observed apparent binding measured using FRET efficiency. B_{max} is the maximum observed FRET efficiency between the donor and the acceptor (labelled proteins binding saturation limit). X is the amount of added binding protein which is inferred from the acceptor to donor ratio. K_d is the apparent binding coefficient, which measures the amount of acceptor to donor ratio observed when the FRET efficiency reaches 50% the B_{max}.

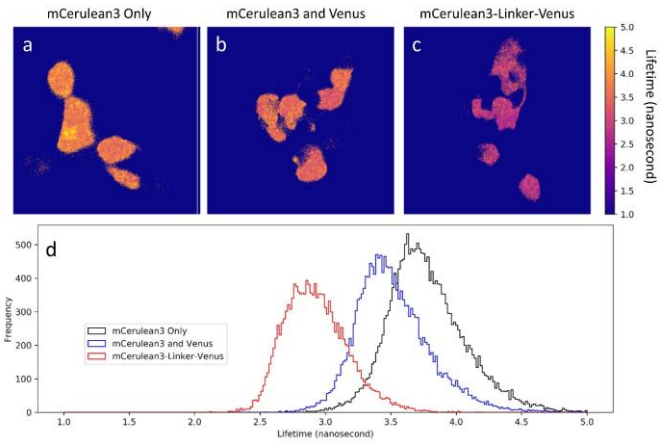

Fig. 5. FLIM imaging of FRET Controls. Lifetime maps of HEK293 expressing mCerulean3 fluorescent protein only (a), mCerulean3 and Venus together (b), and mCerulean3 tethered to Venus using a 13 amino-acids linker (c). (d) shows the lifetime distribution of the three FOVs. The presented maps in (a,,b and c) are a 78×78µm cropped regions of the full FOVs. A threshold mask is applied to remove lifetime estimation for pixel with <20 photons.

IV. Results

Standard dye measurements (Fig. 3) affirm that our system can determine an accurate lifetime within 0.1ns, nevertheless, biologists are not typically interested in measuring dyes in solution. As we mentioned earlier, many biologists are interested in studying protein-protein interactions and the effect of small molecules in live cells. Fluorescence tagged proteins target to membrane structures within the cell, requiring confocality to resolve this useful biological information. We tested the confocality and range of lifetime detection of our system on a standard Convallaria sample (Fig.

4) as well as using live cells expressing donor and acceptor tethered by different size linkers (Fig. 5). Live cell samples are dimmer and more prone to photo-damage than fluorescent standards making this a more relevant model to test the true speed of our system. We determined appropriate exposure settings and measured FRET between two proteins in live MCF-7 cells (Fig. 5). We then determined the number of images required to generate binding curves (Fig 6) and finally, we used our system to evaluate the effectiveness of two small molecule inhibitors (Figure 7). Altogether, these results indicate our multiplexed design is suitable for rapid, confocal FLIM-FRET screening applications.

Photon weighted FLIM confocal image of Convallaria is shown in Fig. 4, which is a confocal scan of the endodermis of the root. The circular structures are vascular bundles of xylem and phloem; different tissues used for transport of water and sugar. These cells tend to have different endogenously fluorescent proteins with different spectral and lifetime properties. A threshold mask is applied, pixels with photon count < 20 are set to zero.

acceptor: donor ratio information is not acquired for a single FOV. The dots with bar are the average and standard deviation for the FRET efficiency at different Acceptor to Donor ratio bins.

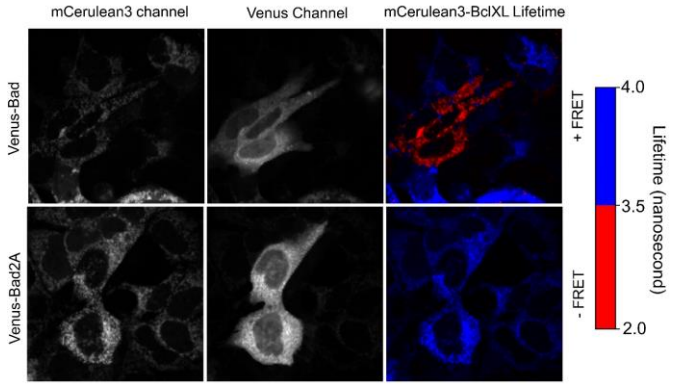

Fig. 6. Confocal FLIM imaging of live MCF-7 stably expressing mCerulean3-BclXL. The top panel shows a zoomed region of cells transiently transfected with Venus-Bad (positive binding control). The bottom panel also shows a magnified region of cells transiently transfected with Venus-Bad2A (negative binding control). In the left panel we see the confocal image for the mCerulean3 channel. In the middle, we see confocal images for the Venus channel. The photon weighted FLIM image of the mCerulean3 is shown in the right panel. The fluorescence lifetime decreases (cells appear in red) when FRET is observed.

V. Discussion

We developed a highly multiplexed confocal microscope (Fig. 1) to perform rapid FLIM imaging. In de-scanning mode, the fluorescence signal is coupled to a SPAD array, which is designed for high temporal acquisitions. Accurate measurement of fluorescence lifetime for the scanned samples required optimization of position and size of the SPAD time-gates (Fig. 2). In our system, we used standard fluorescent dyes to determine these parameters.

A step-and-stop scanning mode is used in the current setup as it is simpler to configure and calibrate but resulted in slower overall scanning acquisition when comparing with resonance scanning mode. Nevertheless, since every focal point is moved across a small distance to the next focal point, the overall time to scan is reduced drastically. We plan to implement resonance scanning in future version of the instrument to further increase acquisition speed.

Using overlapping time-gates of different sizes is recognized as the best gating scheme for estimating lifetime [25]. However, the minimum stable gate size that can be generated by the SPC3 is 2 ns and changing this gate size required updating the internal configurations of the SPC3 detector. To simplify the configuration and make data acquisition less computationally demanding we used two contiguous 4 ns time-gates. Even with our straightforward non-overlapping gating choice, we were able to accurately measure the fluorescence lifetime for Coumarin6 (2.5±0.2 ns) and Fluorescein (4.0±0.2 ns) (Fig. 3 a, b). The excitation light and emission filters are more suitable for imaging Coumarin6, therefore we observed tighter lifetime distribution for Coumarin-6 than Fluorescein (Fig. 3c). However, we note that the tails of both distributions are skewed to overestimate the lifetime (Fig. 3c). This is largely influenced by a few hot pixels in the SPAD array. Punctual defects introduced during the fabrication process lead to large variations in the dark current rate. These non-uniformities ultimately result in an inaccurate estimation of the D_0/D_1 ratio. Our SPC3 prototype contained several faulty pixels that can be spotted in the lifetime maps in Fig. 3 (a) and (b). A typical number of faulty pixels per SPAD detector is in the range of 2-5 per sensor. Non-uniform correction methods have been developed to address these artifacts [26]. Such methods are more appropriately applied in the quality control phase of the SPAD testing. Additional time-gates would also extend the measurable lifetime range [31]. These patches were expected due to differences in the photon detection response from one SPAD pixel to another (Fig. 3a, 3b). Imaging a uniform sample, such as these fluorescent dyes, with a known lifetime allowed for correction of these differences across the detection field (Fig. 4-7).

The fixed *Convallaria* sample (Fig. 4) is bright and has unique structural properties that allow us to determine visually whether each subscan (squares in the images) align with neighboring scans sufficiently. Furthermore, the *Convallaria* sample is typically used to demonstrate the feasibility of the system to measure multiple different lifetimes in the same sample. The measured lifetime observations agree with previously reported values for a *Convallaria* sample [27]. In Figure 4 we observe no 'patching effect' across the entire photon weighted FLIM image, demonstrating that our lifetime and scanner calibration steps (Fig. 2-3) are effective.

Imaging fluorescent proteins in live cells is a more challenging test for the performance of a FLIM microscope, due to the low photon emission compared to fluorescent dyes. We first tested our system using a standard fluorescent protein assay, where we express the donor alone (Fig. 5a), the donor with the acceptor (Fig. 5b) and the donor-fused to-acceptor (Fig. 5c). The previously reported lifetime of mCerulean3 expressed in cells was 3.8±0.3ns. In Figure 5d, the

mCerulean3 and Venus distribution (blue) is visibly shifted compared to mCerulean3 only (black). This is expected, due to the increase in random collisions when the donor and acceptor are expressed in the same cell. However, true FRET resulted in a much larger shift, as seen for the mCerulean3-linker-Venus construct (red compared to black distribution). This demonstrates the feasibility for our system to be used by biologists to measure fluorescent lifetimes of proteins in cells.

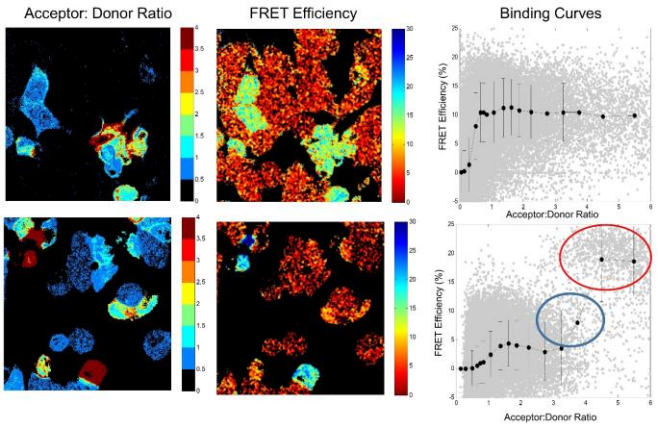

Fig. 7. Binding information extracted from FLIM FRET images for positive and negative binding controls. (left) Acceptor to donor ratio image constructed by dividing acceptor intensity over donor intensity. (center) FRET efficiency map calculated from the lifetime image by comparing to the lifetime of mCerulean3-Bcl-XL without any acceptor. (right) plot of FRET efficiency vs acceptor: donor ratio obtained by plotting the non-zero pixels from FRET efficiency maps(center) and acceptor: donor maps(left). A rapid increase in FRET efficiency, for the negative binding control, is caused by cells overexpressing Venus-Bad2A (red circle). The blue circle highlights the region where acceptor: donor ratio information is not acquired for a single FOV. The dots with bar are the average and standard deviation for the FRET efficiency at different Acceptor to Donor ratio bins.

Unlike these linker constructs, many proteins have restricted localization in the cell. For example, two proteins may both be localized in one organelle, and in that case, we would expect an increase in collisional effects. Consequently, proper controls are required to interpret FLIM-FRET data. Observed changes in lifetime can only be attributed to binding (FRET) with a negative control experiment: a point mutation in the binding site of one of the proteins of interest disrupts binding but maintains the same 'collisional' effects (same localization in the cell) as the wild type protein. In Figures 6-7 we used, Venus-Bad2A (discussed later), as our negative control. If a point mutation is unknown, another non-binding protein with the same localization must be used as a negative control for best practice. This emphasizes that changes in rate of energy transfer, due to having two fluorophores at a proximity to one another, does not necessary indicate binding. Binding is only confirmed when compared to a control for collisions.

In this work, we use the Bcl-2 family proteins as a model system to demonstrate the performance of the confocal FLIM-FRET technique. Bcl-2 family proteins are regulators of cell death (apoptosis). Some Bcl-2 family proteins are pro-apoptotic, while others are anti-apoptotic. On a basic level, interactions between these proteins determine whether a cell dies. Cancer cells can avoid cell death by becoming addicted to overexpression of anti-apoptotic protein(s). Thus, Bcl-2 protein-protein interactions are now the targets of several cancer-therapeutics, called BH3 mimetics: drugs designed to compete for binding anti-apoptotic protein(s). Many BH3 mimetics are now actively being developed, but few have been tested in live cells against full length protein-protein interactions [28]. We foresee the combination of rapid FLIM imaging and high content screening as an indispensable tool to investigate such interactions. We used our system to measure FRET between mCerulean3 (Donor) fused to a protein, Bcl-XL, and Venus (Acceptor) fused to a protein, Bad. These are two members of the Bcl-2 family of proteins, which have been previously shown by FLIM-FRET to bind [24]. Bcl-XL and Bad proteins localize to both the cytosol and mitochondrial outer membrane. For the negative FRET control, we expressed Venus fused to Bad2A, where '2A' indicates two critical residues in the BH3 ligand domain of Bad have been mutated to disrupt binding, as previously reported [29]. In cells Venus-Bad binds to mCerulean3-Bcl-XL and the change in lifetime is captured by our system (Fig. 6). There was no observed change in lifetime with the negative control protein, Venus-Bad2A, as previously published by Liu et al [24].

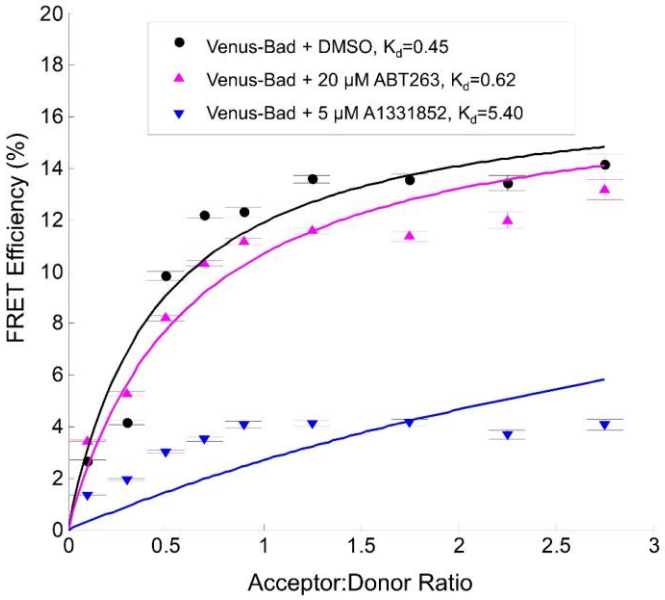

Fig. 8. Effect of two Bcl-2 inhibitors (Abbvie ABT263 and A1331852) on binding between Bcl-XL and Bad. The binding curves were generated by binning data from 4 FOVs. The data points are averages obtained from each bin. The error bars represent the standard error. Each binding curve is fit a single site Hill equation (solid lines) to estimate the apparent Kd. The untransfected well was treated with dilution media (DMSO) used for the drugs to ensure that the media does not change the lifetime of the donor.

For screening applications, binding information must be captured by a fast and easy readout. For this purpose, we generate binding curves and fit the data to get meaningful information (Fig. 7). To fit the data, we convert changes in lifetime to % FRET Efficiency. By comparing the Venus-Bad and Venus-Bad2A curves, we can distinguish binding from collisions. Binding curves are usually generated by combining

data from many Fields of Views (FOVs), for example, Osterlund et al., required 100, 100×100µm images/sample [30]. On our system, we acquired a large 960×960 pixel (310×310µm) two channel FLIM images (mCerulean3 and Venus) in less than 1.5 seconds. We can extract enough information to generate binding curves with as little as 1 FOV (Fig. 7). However, a single FOV may not contain transfected cells that fall in the full range of Acceptor:Donor ratios (for example, Fig. 7, blue circle). Therefore, we recommend taking at least 4 FOV per sample. The 4 images can be acquired in only 6s on our multiplexed system to generate full binding curves. In theory, our system could collect FLIM-FRET binding data for an entire 384-well plate of samples in less than 38 minutes, making it suitable for screening applications.

We used the same binding proteins, Bcl-XL and Bad, to examine two small molecule inhibitors of Bcl-XL, ABT-263 and A-1331852 (Abbvie). Generated binding curves shown in Fig. 8 were fit to a single site Hill slope binding equation to extract the apparent binding dissociation constant (K_d). A lower apparent Kd means higher affinity of binding. The Kd was higher with the addition of A-1331852, compared to ABT-263 or DMSO only. Therefore, A-1331852 is a better inhibitor of this interaction (recently shown in Ref. 29). Altogether, this demonstrates that our system can be used to perform a rapid FLIM-FRET screen for drugs that disrupt specific protein-protein interactions.

ACKNOWLEDGMENT

The SPAD array detector was on loan by Micro Photon Devices (Bolzano, Italy), and Optoelectronics Corporation (Montreal, QC). This project is supported in part by the Natural Science and Engineering Research Council (NSERC) of Canada through its idea-to-innovation (i2i) program (QF). D. W. Andrews holds the Canada Research Chair in Membrane Biogenesis. Q. Fang holds the Canada Research Chair in Biophotonics.

REFERENCES

[1] Y. Feng, Q. Wang, and T. Wang, "Drug target protein-protein interaction networks: a systematic perspective," BioMed research international, vol. 2017, June 2017.

[2] S. Hayes, B. Malacrida, M. Kiely, and P. A. Kiely, "Studying protein–protein interactions: progress, pitfalls and solutions," Biochemical Society Transactions, vol. 44, no. 4, pp. 994–1004, August 2016.

[3] G. Itchaki and J. R. Brown, "The potential of venetoclax (abt-199) in chronic lymphocytic leukemia," Therapeutic advances in hematology, vol. 7, no. 5, pp. 270–287, July 2016.

[4] O. Kepp, L. Galluzzi, M. Lipinski, J. Yuan, and G. Kroemer, "Cell death assays for drug discovery," Nature reviews Drug discovery, vol. 10, no. 3, p. 221, March 2011.

[5] M. J. Wildey, A. Haunso, M. Tudor, M. Webb, and J. H. Connick, "High-throughput screening," in Annual Reports in Medicinal Chemistry. Elsevier, 2017, vol. 50, pp. 149–195.

[6] V. Sharma, T. Ranjan, P. Kumar, A. K. Pal, V. K. Jha, S. Sahni, and B. D. Prasad, "Protein–protein interaction detection: Methods and analysis," in Plant Biotechnology, Volume 1. Apple Academic Press, 2017, pp. 391–411.

[7] M. L. Doyle, "Characterization of binding interactions by isothermal titration calorimetry," Current Opinion in Biotechnology, vol. 8, no. 1, pp. 31 – 35, February 1997.

[8] P. Singh, "Spr biosensors: historical perspectives and current challenges," Sensors and actuators B: Chemical, vol. 229, pp. 110–130, June 2016

[9] W. R. Algar, N. Hildebrandt, S. S. Vogel, and I. L. Medintz, "FRET as a biomolecular research tool—understanding its potential while avoiding pitfalls," Nature methods, vol. 16, no. 9, pp. 815–829, August 2019.

[10] A. Elder, A. Domin, G. Kaminski Schierle, C. Lindon, J. Pines, A. Esposito, and C. Kaminski, "A quantitative protocol for dynamic measurements of protein interactions by Fo¨rster resonance energy transfersensitized fluorescence emission," Journal of The Royal Society Interface, vol. 6, no. suppl 1, pp. S59–S81, November 2008.

[11] T. Karpova and J. G. McNally, "Detecting protein–protein interactions with cfp-yfp fret by acceptor photobleaching," Current protocols in cytometry, vol. 35, no. 1, pp. 12–7, February 2006.

[12] K. Suhling, P. M. French, and D. Phillips, "Time-resolved fluorescence microscopy," Photochemical & Photobiological Sciences, vol. 4, no. 1, pp. 13–22, January 2005.

[13] D. M. Shotton, "Confocal scanning optical microscopy and its applications for biological specimens," Journal of Cell Science, vol. 94, no. 2, pp. 175–206, May 1989.

[14] W. F. An and N. Tolliday, "Cell-based assays for high-throughput screening," Molecular biotechnology, vol. 45, no. 2, pp. 180–186, February 2010.

[15] S. P. Poland, N. Krstaji´c, S. Coelho, D. Tyndall, R. J. Walker, V. Devauges, P. E. Morton, N. S. Nicholas, J. Richardson, D. D.-U. Li et al., "Time-resolved multifocal multiphoton microscope for high speed fret imaging in vivo," Optics letters, vol. 39, no. 20, pp. 6013–6016, October 2014.

[16] N. Hirmiz, A. Tsikouras, E. J. Osterlund, M. Richards, D. W. Andrews, and Q. Fang, "Multiplexed confocal microscope with a refraction window scanner and a single-photon avalanche photodiode array detector," Optics Letters, vol. 45, no. 1, pp. 69–72, January 2020.

[17] J. Pawley, Handbook of biological confocal microscopy. Springer Science & Business Media, 2010.

[18] A. Margineanu, J. J. Chan, D. J. Kelly, S. C. Warren, D. Flatters, S. Kumar, M. Katan, C. W. Dunsby, and P. M. French, "Screening for protein-protein interactions using f¨orster resonance energy transfer (FRET) and fluorescence lifetime imaging microscopy (FLIM)," Scientific reports, vol. 6, p. 28186, June 2016.

[19] N. Hirmiz, A. Tsikouras, E. J. Osterlund, M. Richards, D. W. Andrews, and Q. Fang, "Cross-talk reduction in a multiplexed synchroscan streak camera with simultaneous calibration," Optics express, vol. 27, no. 16, pp. 22602–22614, July 2019.

[20] A. Tsikouras, R. Berman, D. W. Andrews, and Q. Fang, "High-speed multifocal array scanning using refractive window tilting," Biomedical optics express, vol. 6, no. 10, pp. 3737–3747, September 2015.

[21] D. Bronzi, F. Villa, S. Tisa, A. Tosi, F. Zappa, D. Durini, S. Weyers, and W. Brockherde, "100 000 frames/s 64× 32 single-photon detector array for 2-d imaging and 3-d ranging," IEEE journal of selected topics in quantum electronics, vol. 20, no. 6, pp. 354–363, August 2014.

[22] M. Liu, M. Jia, H. Pan, L. Li, M. Chang, H. Ren, F. Argoul, S. Zhang, and J. Xu, "Instrument response standard in time-resolved fluorescence spectroscopy at visible wavelength: quenched fluorescein sodium," Applied spectroscopy, vol. 68, no. 5, pp. 577–583, May 2014.

[23] E. J. Osterlund, N. Hirmiz, C. Tardif, and D. W. Andrews, "Rapid imaging of bcl-2 family interactions in live cells using FLIM-FRET," in BCL2 Family Proteins. Springer, 2019, pp. 305–335.

[24] Q. Liu, B. Leber, and D. W. Andrews, "Interactions of pro-apoptotic bh3 proteins with anti-apoptotic bcl-2 family proteins measured in live mcf-7 cells using FLIM FRET," Cell Cycle, vol. 11, no. 19, pp. 3536–3542, August 2012.

[25] H. Gerritsen, M. Asselbergs, A. Agronskaia, and W. Van Sark, "Fluorescence lifetime imaging in scanning microscopes: acquisition speed, photon economy and lifetime resolution," Journal of microscopy, vol. 206, no. 3, pp. 218–224, June 2002.

[26] E. Vilella, J. Garcia, O. Alonso, and A. Dieguez, "Dynamic Range Extension of a SPAD Imager Using Non-Uniformity Correction Techniques," IEEE Sensors Journal, vol. 16, no. 9, pp. 2988-2992, January 2016.

[27] A. Esposito and A. R. Venkitaraman, "Enhancing biochemical resolution by hyperdimensional imaging microscopy," BiophysicalJournal, vol. 116, no. 10, pp. 1815 – 1822, May 2019

[28] J. Kale, E. J. Osterlund, and D. W. Andrews, "Bcl-2 family proteins:changing partners in the dance towards death," Cell Death & Differentiation, vol. 25, no. 1, pp. 65–80, April 2018.

[29] Q. Liu, E. J. Osterlund, X. Chi, J. Pogmore, B. Leber, and D. W. Andrews, "Bim escapes displacement by bh3-mimetic anti-cancer drugs by double-bolt locking both bcl-xl and bcl-2," eLife, vol. 8, p. e37689, Mar 2019.
[30] E. J. Osterlund, Q. Liu, and D. W. Andrews, The Use of FLIM-FRET for the Detection of Mitochondria-Associated Protein Interactions. New York, NY: Springer New York, 2015, pp. 395–419.
[31] Zhu, S., Xu, Y., & Li, D. Three-observation-window time-gated algorithm for fluorescence lifetime detection. Applied Optics, 59(9), 2739-2745, 2020

Nehad Hirmiz received his B.Sc in Physics and Chemistry from the University of Toronto in 2011. He then received his M.Sc. in Biophysics (2014) and PhD in Biomedical Engineering (2019) at McMaster University.

Dr. Hirmiz is currently working as a postdoctoral fellow at the Robarts Research Institute and St. Michael's Hospital, Toronto where he is using deep learning approaches to predict disease progression for patients with Age Related Macular Degeneration.

Anthony Tsikouras received his BEng and PhD in Engineering Physics from McMaster University in 2010 and 2017, respectively.

Dr. Tsikouras is currently with L3 Communications.

Morgan Richards received his B.Sc in Physics from McMaster University in 2018. He is currently a Ph.D. student in the Department of Engineering Physics at McMaster University.

Morgan's research interests include advanced microscopic imaging systems and their applications.

Elizabeth J. Osterlund received her B.Sc in biochemistry from McMaster University in 2012. She is currently a Ph.D. candidate in the Department of Biochemistry at the University of Toronto.

Elizabeth's studies mechanisms by which the Bcl-2 family of proteins regulate selective programmed cell death (apoptosis) of cancer cells. Her research interests include high-content screening, tissue culture techniques and fluorescent microscopy.

David W. Andrews is a Professor of Medical Biophysics in the University of Toronto and a Senior Scientist at the Sunnybrook Health Science Center. Dr. Andrews received his BSc in biochemistry from the University of Ottawa in 1979 and his PhD in medical biophysics from the University of Toronto in 1985. He holds the Canada Research Chair in Membrane Biogenesis.

Dr. Andrews' research interests include cancer chemotherapy, the molecular mechanisms by which Bcl-2 family proteins regulate apoptosis, the assembly of proteins into the cellular membranes, high-content screening, the development of new fluorescence microscopes and automated image analysis techniques.

Qiyin Fang is a Professor of Engineering Physics and Canada Research Chair in Biophotonics at McMaster University. He received his BSc in Physics from Nankai University, and both his MSc. in Applied Physics and PhD in Biomedical Physics from East Carolina University. He worked at Cedars-Sinai Medical Center in Los Angeles before moving to McMaster.

Dr. Fang's current research interests include optical spectroscopy and imaging for minimally invasive diagnosis and guided therapy, miniaturized sensors and imaging systems, advanced optical microscopy, and smart sensing systems for aging-in-place and environmental applications. Dr. Fang is a Fellow of SPIE.